OPTIMIZATION OF SUPERSONIC AXISYMMETRIC NOZZLES WITH A CENTER BODY FOR AEROSPACE PROPULSION

D. M. Davidenko,* Y. Eude,* and F. Falempin†

*ICARE – Institut de Combustion, Aérothermique, Réactivité et Environnement, CNRS

1C Avenue de la Recherche Scientifique, 45071 Orléans, France

†MBDA France

1 Avenue Réaumur, 92358 Le Plessis Robinson, France

ABSTRACT

This study is aimed at optimization of axisymmetric nozzles with a center body, which are suitable for thrust engines having an annular duct. To determine the flow conditions and nozzle dimensions, the Vinci rocket engine is chosen as an example. The nozzle contours are described by 2nd and 3rd order analytical functions and specified by a set of geometrical parameters. A direct optimization method is used to design maximum thrust nozzle contours. During optimization, the flow of multispecies reactive gas is simulated by an Euler code. Several optimized contours have been obtained for the center body diameter ranging from 0.2 m to 0.4 m. For this contours, Navier-Stokes simulations have been made to take into account viscous effects assuming adiabatic and cooled wall conditions. The paper presents an analysis of factors influencing the nozzle thrust.

INTRODUCTION

Particular concepts of aerospace engines, e.g. continuous detonation wave engine [1], have an annular combustion chamber and require a supersonic nozzle with a center body for compatibility. To provide the maximum thrust for given geometric limitations (length and diameter), the nozzle contour must be carefully optimized. The modern approach to the nozzle design and optimization and related problems are discussed in [2].

Since the early works of Rao [3, 4] on the optimization of bell and spike nozzle contours, a significant effort has been made to apply the nozzle optimization, based on the calculus of variations and the method of characteristics, to flows with viscous boundary layers [5] and chemically nonequilibrium flows [6]. At the same time, applicability of direct optimization methods together with a simple analytical description of nozzle contour was proved [7].

Being well adapted to the design of several standard aerodynamic shapes, the method of characteristics is relatively difficult to generalize for an arbitrary form. Finite-volume methods based on shock capturing numerical schemes are much more flexible in this respect. In this paper, a direct optimization method is used in combination with a 2D Euler code to design maximum thrust nozzle contours.

PROBLEM FORMULATION AND NUMERICAL METHODS

Nozzle geometry

For an annular nozzle, each wall contour is considered as a circular arc followed by a 2nd or 3rd order parabolic curve as shown in Fig. 1. For the lower (index “L”) and upper (index “U”) contours, the following parameters are specified:

- starting point coordinates, x_{inl} and y_{inl};
- circular arc radius, R;
- contour angle at the attachment point, β_{att};

- limiting coordinates, x_{end} and y_{end};
- parabolic contour abscissa, x_{par}, on the line $y = y_{end}$;
- tangent angle, β_{par}, at the point (x_{par}, y_{end}).

This parameter set is sufficient to define a parabolic contour passing through the points (x_{att}, y_{att}) and (x_{par}, y_{end}) with the β_{att} tangent angle. β_{par} is used as a parameter if the upper contour is described by a cubic parabola. If $x_{par} < x_{end}$, the contour is limited by the radial coordinate, y_{end}. If $x_{par} > x_{end}$, the contour is limited by the axial coordinate, x_{end}.

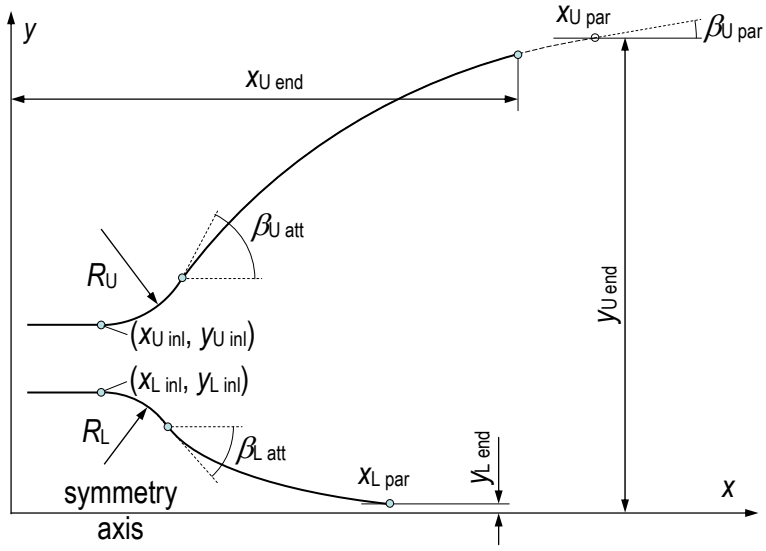

Fig. 1: Schematic of the nozzle contour.

Flow simulation methods

A steady-state nozzle flow is simulated in 2D axisymmetric configuration using either the Euler or Navier-Stokes approach. Most of the Euler simulations have been made with a particular code that realizes a 2nd order accurate space-marching scheme. The space marching is performed along the principal flow direction. An implicit Runge-Kutta integration scheme is applied to ensure a robust solution procedure for a chemically reacting flow. The computational mesh is automatically generated during each simulation. It has 50 points in the *y*-direction uniformly distributed and arranged along parallel vertical lines. The mesh step in the *x*-direction is controlled by a given Courant number. Numerical tests have shown that the integral pressure forces applied to the nozzle are practically independent (to 0.01%) of the Courant number variation within the range 0.5-2 and are the same for a twice denser mesh in the *y*-direction.

Navier-Stokes simulations as well as some Euler simulations have been performed with the Fluent® 6.3 commercial code. Implicit integration and a 2nd order accurate space approximation are chosen for the solution procedure. A structured mesh has 70 cells in the transversal direction and the cell number in the longitudinal direction is of the order of 500. The mesh is clustered near the walls in order to properly resolve the boundary layers. The minimum cell size is about 60-70 μm.

A finite-rate kinetic model is adopted to describe the non-equilibrium chemistry during the combustion product expansion. This model is represented by a kinetic mechanism including 6 species (H_2, O_2, H_2O, H, O, and OH) and 7 reversible chemical reactions [8]. For pure species, temperature-dependent thermodynamic properties are described by standard polynomials [9].

The molecular viscosity and conductivity of the gaseous mixture are evaluated according to the kinetic theory [10] and approximated as temperature functions under the following assumptions: the mixture is at chemical equilibrium whereas the temperature and pressure are isentropically related.

Species diffusivities are considered with respect to fully recombined combustion products, containing only major species, and approximated as functions of the pressure and temperature.

As a turbulence model, the Wilcox k-ω model [11] is used together with the compressibility correction. The turbulent Prandtl and Schmidt numbers are taken equal to 0.85.

Nozzle contour optimization

An automatic optimization procedure specifies the nozzle contour, for which the flow is simulated by the marching Euler code. The optimization procedure operates on maximum 4 parameters:

- $\beta_{L\,att}$ and $x_{L\,par}$ for the lower contour, which is always quadratic;
- $\beta_{U\,att}$ and $x_{U\,par}$ for the quadratic upper contour or $\beta_{U\,att}$ and $\beta_{U\,par}$ for the cubic upper contour.

The optimization algorithm is based on the alternate-direction method with simple restrictions on the optimization parameters. The x-component of the pressure force, integrated along the lower and upper contours, are included in the optimization criterion.

Engine specifications

In the present study, the optimization method is applied to an annular nozzle, for which the nozzle of the Vinci rocket engine is taken as a prototype. From publications made by Astrium and Snecma, the following data are fixed for the study:

- nozzle exit diameter 2.15 m
- mass flow rate 33.7 kg/s
- chamber pressure 6.08 MPa
- mixture ratio O_2/H_2 5.84

From available photos of the engine, we could roughly estimate longitudinal dimensions of the diverging nozzle:

- length of the fixed part 1.4 m
- total deployed length 3.4 m

The throat area, the flow conditions in the throat section, and the ideal engine performance have been obtained from ideal equilibrium simulations.

- throat diameter 0.1323 m
- total pressure 5.781 MPa
- static pressure 3.334 MPa
- total temperature 3529 K
- static temperature 3340 K
- velocity 1548 m/s
- engine specific impulse 4842 m/s 4581 m/s (official data)
- engine vacuum thrust 163.2 kN 155 kN (official data)
- supersonic nozzle thrust 65.2 kN

For most of the cases considered below, the circular arc radii, R_U and R_L, are taken equal to the throat diameter. Different diameters of the center body chosen for the optimization are D_{CB} = 0, 0.2, 0.3, and 0.4 m. The nozzle length, $x_{U\,end}$, is limited to 3.4 m and the center body length to 1.4 m (length of the fixed part of the nozzle).

Boundary conditions

For the nozzle flow simulation, a uniform sonic flow is imposed in the inlet cross section. This is a 1st order approximation. The sonic line is usually curved [12] and its exact form depends on the duct configuration upstream from the nozzle throat that we do not consider in the present study. The gas composition at the inlet corresponds to the chemical equilibrium and is specified in terms of species mass fractions in Table 1. One can appreciate the dissociation level noting that the composition of filly recombined combustions products is 0.96138 of H_2O and 0.03862 of H_2.

Table 1: Species mass fractions at the inlet

H_2O	H_2	O_2	OH	H	O
0.89866	0.04008	0.00704	0.04789	0.00272	0.00361

For the Navier-Stokes simulations, a turbulence intensity of 5 % and a turbulence length scale of 0.5 mm are imposed at the inlet. No slip conditions are used for the flow velocity on the walls. Two kinds of thermal wall conditions are considered: adiabatic and constant temperature of 1300 K.

The outflow conditions are without importance as the flow velocity is supersonic everywhere in the exit cross section.

RESULTS AND DISCUSSION

Validation of the optimization method

A first test is related to the classical bell nozzle. A nonreacting perfect gas is considered with the following properties: ratio of specific heats 1.2; gas constant 630 J/(kg K). The aforementioned static pressure and temperature in the throat are imposed together with a Mach number of 1.01. The nozzle contour is designed using several methods: the method of characteristics [12], optimum quadratic contour, and optimum cubic contour. For the method of characteristics, the circular contour upstream from the attachment point is fixed whereas the downstream contour is designed along a streamline. The $\beta_{U\,att}$ angle is adjusted to obtain a contour passing through the point ($x_{U\,end}$ = 3.4 m, $y_{U\,end}$ = 1.075 m). It should be noted that the end point has the same coordinates in the other cases. The results are summarized in Table 2.

Table 2: Contour angles and normalized thrust for the classical nozzle

	Characteristics	Quadratic optimum	Cubic optimum
$\beta_{U\,att}$, deg	32.1	40.3	36.1
$\beta_{U\,par}$, deg	8.0*	10.1*	8.2
F_N/F^*_N#	0.9829	0.9816	0.9857

*Non-optimized angle.

#Nozzle thrust normalized by the ideal nozzle thrust 63 kN in the perfect gas case.

One can note that the angles obtained for the quadratic contour are significantly different from the corresponding values provided by the method of characteristics. The optimum cubic contour is in closer agreement with the method of characteristics and it gives a higher thrust. The three contours are plotted in Fig. 2.

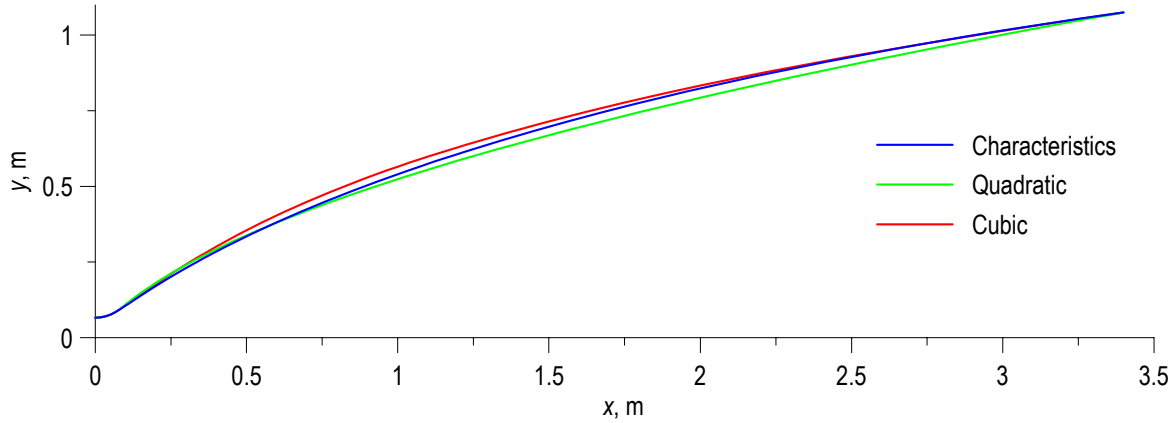

Fig. 2: Comparison of nozzle contours obtained for the classical configuration.

Factors influencing the thrust

The nozzle thrust, F_N, can be considered as a sum of the integral pressure force and the skin friction drag acting in the *x*-direction. The most important factors that influence these integral forces are the contour form, chemical reactions, and wall thermal conditions. The contribution of each factor can be assessed from the following consideration. 0D equilibrium computations provide the highest theoretical level for the nozzle thrust F^*_N = 65.2 kN and the engine thrust F^*_E =163.17 kN. By progressively increasing the complexity of the numerical approach and choosing different options, it is possible to evaluate the influence of each factor more or less independently. Results obtained for the classical configuration are given in Table 3. The figures represent differences of the pressure force, $\Delta F_p = F_p - F^*_N$, nozzle thrust, $\Delta F_N = F_N - F^*_N$, and engine thrust, $\Delta F_E = F_E - F^*_E$, as well as the viscous force, F_v, with respect to the highest theoretical thrust.

Table 3: Influence of different factors on the nozzle and engine thrust

Approach	Chemistry	Form	Wall	$\Delta F_p / F^*_N$ (%)	F_v / F^*_N (%)	$\Delta F_N / F^*_N$ (%)	$\Delta F_E / F^*_E$ (%)
0D	Frozen			–12.1		–12.1	–4.8
1D	Finite rate	Conical		–0.7		–0.7	–0.3
2D Euler	Finite rate	Conical		–5.3		–5.3	–2.1
		Cubic		–2.0		–2.0	–0.8
2D NS	Finite rate	Cubic	Adiabatic	0.7	–5.2	–4.5	–1.8
			T_w = 1300 K	–0.7	–5.8	–6.5	–2.6

The most important losses are obtained if the gas composition is frozen in the nozzle but this is not a real case. With the finite-rate chemistry, the nozzle thrust losses are within 1 %. Independently of the numerical approach and the nozzle form, the mean mass fraction of H_2O in the exit cross section is about 0.961 i.e. close to the equilibrium. Due to the nozzle form, the trust losses increase by 1.3-4.6 %. As compared to the conical nozzle, more than 3 % of thrust can be gained if the nozzle contour is optimized. With the viscous effects, the flow is less expanded thus the pressure force increases with respect to the inviscid case. However, the net effect is negative because the skin friction drag represents more than 5 % of the nozzle thrust. Finally the wall cooling is responsible for a 2 % nozzle thrust loss due to the pressure force reduction and viscous force increase.

Contours optimization for inviscid flow

This section presents results for a nonequilibrium inviscid flow in the nozzle. A parametric study has been conducted for D_{CB} = 0.4 m and both shapes of the upper contour. In the case of nozzle with quadratic upper contour, all the four optimization parameters are varied. It is found that the maximum thrust is always obtained when $x_{U\,par} = x_{U\,end}$. The effect of the other parameters, $x_{L\,par}$, $\beta_{L\,att}$, and $\beta_{U\,att}$, is illustrated in Fig. 3 for the normalized nozzle thrust, F_N, and its constituents corresponding to the lower contour, F_L, and the upper contour, F_U. F_L, is independent of $\beta_{U\,att}$ within the considered domain. For a constant lower angle, $\beta_{L\,att}$, the greatest F_L is found on the boundary corresponding to a straight line. The shortest straight contour is the best one to maximize F_L. However, this is not the case for F_U, for which the greatest value is found for the longest possible center body with a straight contour ($x_{L\,par}$ = 1.4 m). The nozzle total thrust, F_N, exhibits a similar behavior. One can conclude from this analysis that the variation of the center body shape makes a stronger effect on F_U than on F_L.

In the case of nozzle with cubic upper contour, both contour lengths are fixed: $x_{L\,par}$ = 1.4 m and $x_{U\,par}$ = 3.4 m. The effect of the contour angles, $\beta_{L\,att}$, $\beta_{U\,att}$, and $\beta_{U\,par}$, on F_L, F_U, and F_N is illustrated in Fig. 4. Once again, the variation of $\beta_{L\,att}$ acts in opposite ways on F_L and F_U. As in the previous case, the maximum nozzle thrust is obtained for the straight center body contour. One can see an optimum of F_N in the plain $\beta_{U\,att}$-$\beta_{U\,par}$ at $\beta_{L\,att}$ = –7.78°.

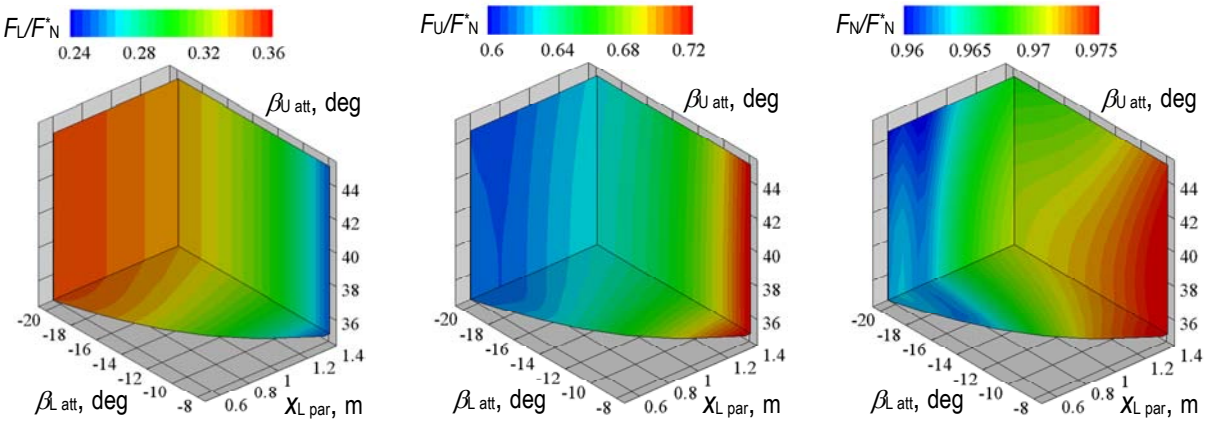

a) b) c)

Fig. 3: Normalized pressure forces for D_{CB} = 0.4 m and quadratic upper contour: lower contour (a), upper contour (b), and their sum (c).

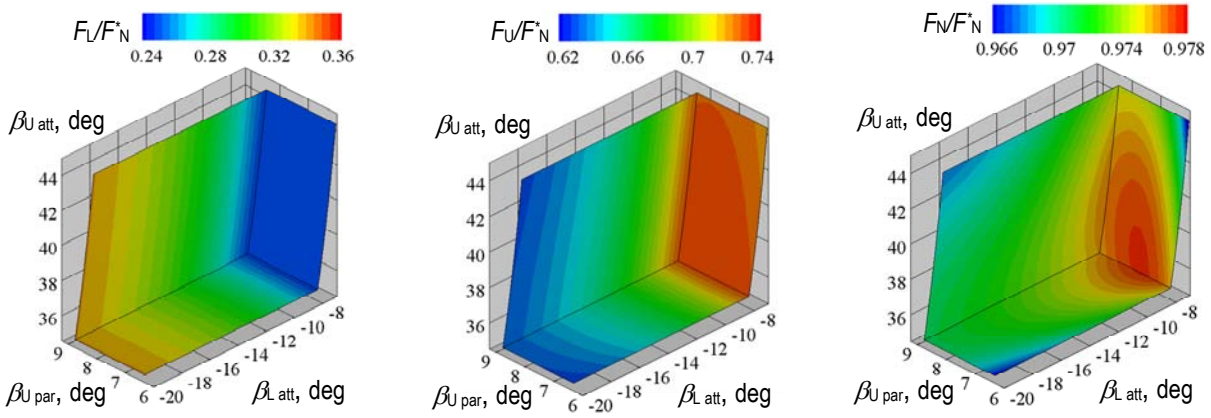

a) b) c)

Fig. 4: Normalized pressure forces for D_{CB} = 0.4 m and cubic upper contour: lower contour (a), upper contour (b), and their sum (c).

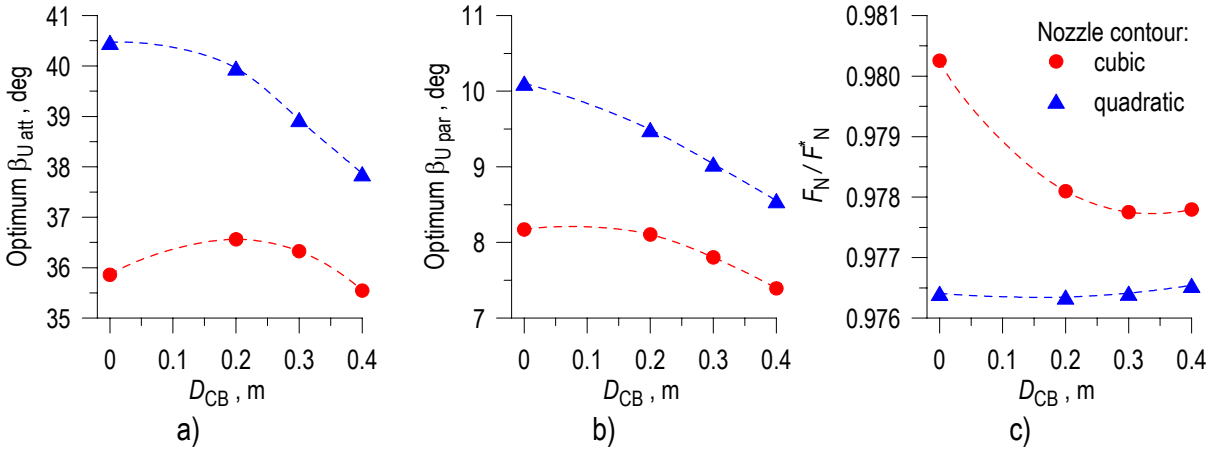

a) b) c)

Fig. 5: Optimum contour angles (a, b) and normalized nozzle thrust (c) versus center body diameter for quadratic and cubic upper contours.

Optimum nozzle shapes have been designed for different diameters of the center body. The best shape of the center body contour is always straight with the maximum allowed length, $x_{L\,par}$ = 1.4 m. In Fig. 5, optimum values of $\beta_{U\,att}$ and $\beta_{U\,par}$ and corresponding normalized thrust, F_N/F^*_N, are plotted

versus D_{CB} for quadratic and cubic upper contours. One can note that the cubic contour has always lesser angles $\beta_{U\,att}$ and $\beta_{U\,par}$ than the quadratic one. Within the range D_{CB} = 0.2-0.4 m, optimum angles demonstrate decreasing trends for both contour kinds. Thrust obtained with a center body is slightly lower with respect to the classical nozzle (D_{CB} = 0) in the case of cubic contour and independent of D_{CB} in the case of quadratic contour. The overall thrust difference is 0.15-0.4 %.

According to the results presented in Fig. 4, the maximum thrust corresponds to the limiting case for the center body having a straight contour. This suggests an idea to try ogive forms, for example, a fully circular contour or contours with a cylindrical portion, as shown in Fig. 6 for D_{CB} = 0.4 m. The length of the cylindrical portion, L_{cyl}, corresponds to $x_{L\,inl}$ in Fig. 1. It should be noted that the optimum upper contour is sensitive to the center body shape up to $x_L \approx 0.6$ m. Beyond this length, the center body shape is important only for the force applied to the lower contour, F_L.

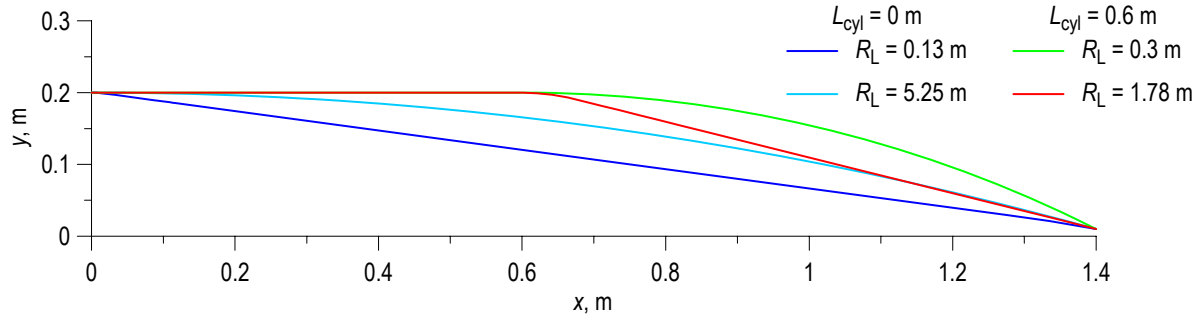

Fig. 6: Various ogive forms of the center body for D_{CB} = 0.4 m.

Nozzle optimization has been performed for center bodies with a cylindrical portion and two shapes of the converging portion: straight with relatively small R_L and circular with maximum possible R_L. Results obtained for variable L_{cyl} and different D_{CB} are shown in Fig. 7. Optimum values of $\beta_{U\,att}$ are practically equal to 38° for all cases except for the straight contour with L_{cyl} =0 and 0.1 m. One can see in Fig. 7b that the fraction represented by F_L in the nozzle thrust drastically reduces when L_{cyl} increases. This is because the converging portion of the center body shifts toward the low pressure zone. Nevertheless, the nozzle thrust increases due to the rise of F_U. Depending on D_{CB}, maximum thrust is obtained at L_{cyl} =0.4-0.5 m. The circular shape is better at lesser L_{cyl} whereas the straight shape has an advantage at greater L_{cyl}. One can also note that with an ogive center body the maximum thrust exceeds the level corresponding to the classical nozzle (see Fig. 7c).

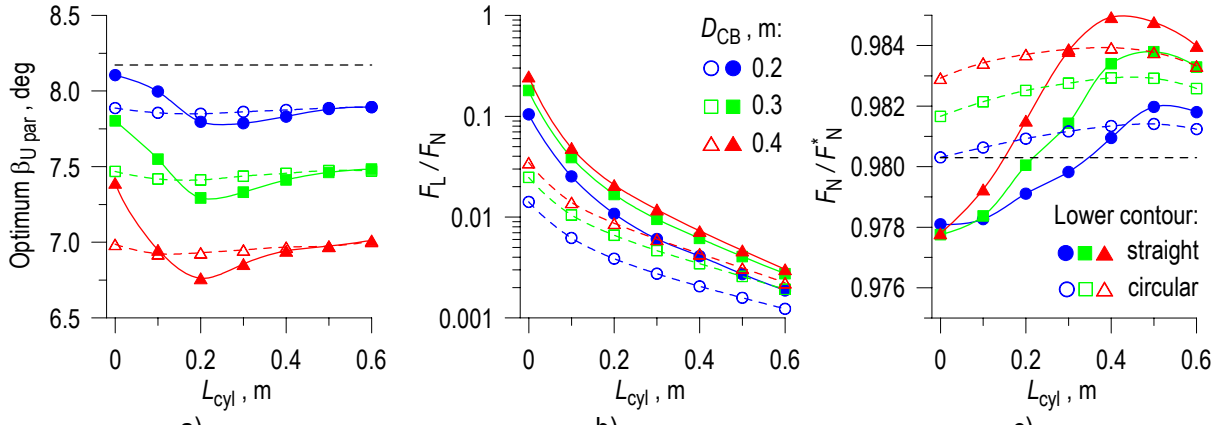

Fig. 7: Optimum contour angle at the end point (a), F_L fraction in the nozzle thrust (b), and normalized nozzle thrust (c) versus length of the center body cylindrical portion. Horizontal line marks the level corresponding to the classical nozzle.

Nozzle thrust with viscous losses

From the previous analysis of thrust losses, one can see that viscous effects represent a very important factor that must be taken into account to choose the best nozzle contour. This subsection provides an analysis based on results of Navier-Stokes simulations performed for several optimized contours.

The nozzles with cubic upper contours and straight lower contours, for which optimization results are presented in Fig. 5, will be considered first. For these nozzles, Euler and Navier-Stokes results on $F_{p\,N}/F^*_N$, $F_{v\,N}/F^*_N$, and F_N/F^*_N as functions of D_{CB} are shown in Fig. 8. $F_{p\,N}$ and $F_{v\,N}$ respectively represent total pressure and viscous forces integrated along the lower and upper contours. The nozzle thrust is defined as $F_N = F_{p\,N} + F_{v\,N}$. Navier-Stokes results are given for the cases of adiabatic and cooled walls. With respect to the Euler simulations, $F_{p\,N}$ is 1 % to 4 % higher because the flow expansion in the nozzle is reduced by the growing boundary layers. Accounting for $F_{v\,N}$ that represents –5 % to –8 %, net losses in F_N are 2.6-3 % for adiabatic walls and 4.6-6.2 % for cooled walls (higher losses correspond to larger D_{CB}).

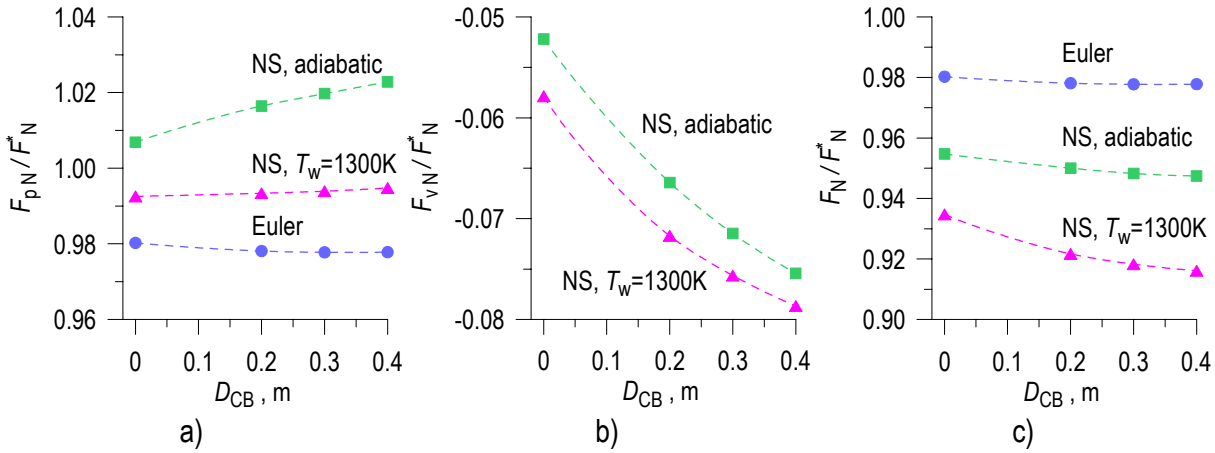

Fig. 8: Normalized total pressure force (a), total viscous force (b), and nozzle thrust (c) versus diameter of the center body from Euler and Navier-Stokes (NS) simulations.

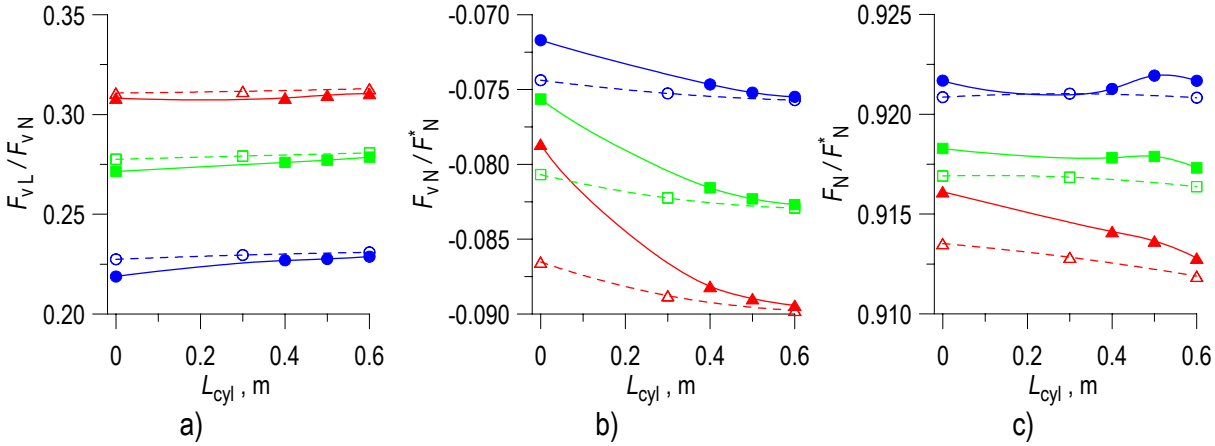

Fig. 9: Fraction of the center body viscous force in the total viscous force (a), normalized total viscous force (b), and normalized nozzle thrust (c) versus length of the center body cylindrical portion. The legends are given in Fig. 7.

Navier-Stokes results, corresponding to ogive forms of the center body (see Figs. 6 and 7), are shown in Fig. 9. $F_{v\,L}/F_{v\,N}$, $F_{v\,N}/F^*_N$, and F_N/F^*_N are plotted versus L_{cyl} for different diameters D_{CB} = 0.2-0.4 m. $F_{v\,L}$ is the viscous force applied to the lower contour. One can note that the center body creates a drag, which represents an almost constant fraction of $F_{v\,N}$ when L_{cyl} increases. The net force $F_L = F_{p\,L}$ +

$F_{v\,L}$ is negative at $L_{cyl} \geq 0.3$ m. Ogive forms with circular converging portion provide much more important drag at $L_{cyl} = 0$. As a result, these forms have no advantage at any L_{cyl}. Ogive forms with straight converging portion can give a little better performance at $D_{CB} = 0.2$ m and are definitely disadvantageous at $D_{CB} = 0.4$ m. Taking into account the weight and wall cooling, the case of straight contour with $L_{cyl} = 0$ should be finally preferred.

Nozzle flowfield

To illustrate the nozzle flowfield, Mach number fields are shown in Figs. 10 for two center bodies with straight contours: $D_{CB} = 0.2$ m and 0.4 m. Flowfields above and below the axis respectively correspond to the Euler and Navier-Stokes simulations. The boundary layers on the nozzle walls are clearly seen. The displacement effect, which reduces flow expansion, is manifested by lower Mach numbers toward the nozzle exit. Because of the flow convergence near the center body, a conical shock front is formed downstream from its tip. This shock is visible in the Mach fields obtained from the Euler simulations. The Navier-Stokes results show that the flow convergence leads to a quick growth of the boundary layer on the center body. This results in a wake in the free flow around the axis and suppresses the conical shock.

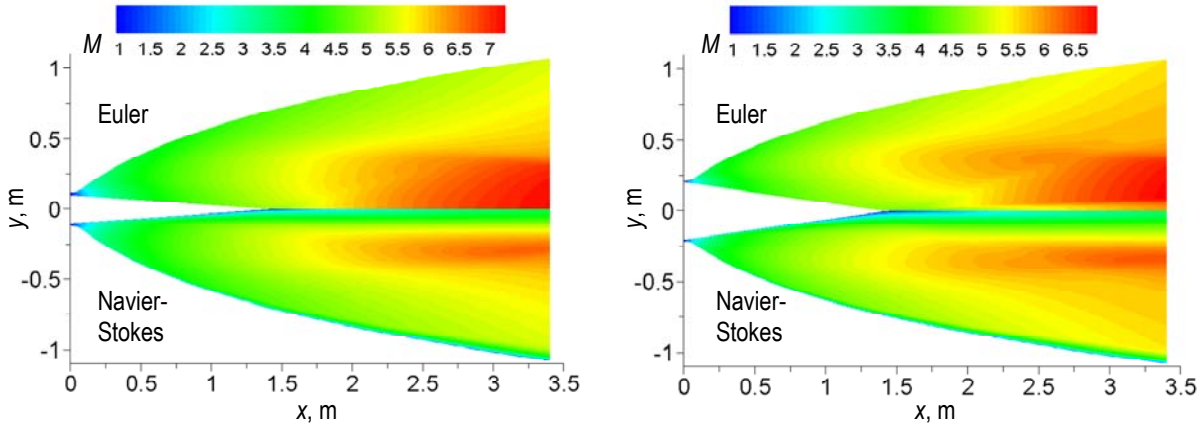

a) b)

Fig. 10: Mach number fields for $D_{CB} = 0.2$ m (a) and 0.4 m (b) from Euler (above axis) and Navier-Stokes (below axis) simulations.

CONCLUSIONS

A numerical study has been conducted to determine optimum shapes of axisymmetric nozzles with a center body. Several optimized contours have been designed based on Euler simulations for different diameters and forms of the center body. The highest thrust is obtained for an ogive form consisted of a cylindrical part and a straight converging part.

For the optimized contours, Navier-Stokes simulations have been performed in order to take into account viscous losses due to the skin friction and heat exchange. According to the obtained results, the viscous effects are responsible for a 3 % to 6 % thrust reduction with respect to the Euler results. Among the considered configurations of the center body, the case of straight contour without cylindrical part should be finally preferred.

ACKNOWLEDGMENT

The financial support of MBDA-France, the Centre National de la Recherche Scientifique (CNRS), the FEDER and FSE funds of the European Commission, the Region Centre, the Departement of Cher, the Communauté d'Agglomeration Bourges Plus, and the Prefecture of Region Centre is greatly acknowledged.

REFERENCES

[1] Bykovskii, F. A., Zhdan, S. A., and Vedernikov, E. F., “Continuous spin detonations,” Journal of Propulsion and Power, Vol. 22, 2006, pp. 1204-1216.
[2] Vuillermoz, P., Weiland, C., Hagemann, G., Aupoix, B., et al., “Nozzle desing and optimization,” in “Liquid rocket thrust chambers: aspects of modeling, analysis, and design,” V. Yang, M. Habiballah, J. Hulka, and M. Popp (eds.), Progress in aeronautics and astronautics, Vol. 200, 2004, pp. 469-492.
[3] Rao, G. V. R., “Exhaust nozzle contour for optimum thrust,” Jet Propulsion, Vol. 28, No. 6, 1958, pp. 377-382.
[4] Rao, G. V. R., “Spike nozzle contour for optimum thrust,” in “Ballistic missile and space technology”, Vol. 2, C. W. Morrow (ed.), Pergamon Press, New York, 1961.
[5] Hoffman, J. D., Scofield, M. P., and Thompson, H. D., “Thrust nozzle optimization including boundary layer effects,” Journal of Optimization Theory and Applications, Vol. 10, No. 3, 1972, pp. 133-159.
[6] Hoffman, J. D., “A general method for determining optimum thrust nozzle contours for chemical reacting gas flows,” AIAA Journal, Vol. 5, No. 4, 1967, pp. 670-676.
[7] Allman, J. G. and Hoffman, J. D., “Design of maximum thrust nozzle contours by direct optimisation methods,” AIAA Journal, Vol. 19, No. 6, 1981, pp. 750-751.
[8] Davidenko, D. M., Gökalp, I., Dufour, E., and Magre, P., “Systematic numerical study of the supersonic combustion in an experimental combustion chamber,” 14th AIAA/AHI Space Planes and Hypersonic Systems and Technologies Conference, AIAA-2006-7913, Canberra, 6-9 Nov. 2006.
[9] Burcat, A. and Ruscic B., Report No. ANL-05/20, Argonne National Laboratory, Report No. TAE 960, Technion, 2005.
[10] Bird, R. B., Stewart, W. E., and Lightfoot, E. N., “Transport phenomena,” John Wiley and Sons, New York, 1960.
[11] Wilcox, D. C., “Turbulence modeling for CFD,” 2nd edition, DCW Industries, Inc., 1998.
[12] Zucrow, M. J. and Hoffman, J. D., “Gas dynamics,” Vol. II, John Wiley and Sons, New York, 1977.